nature geoscience

ARTICLES

PUBLISHED ONLINE: 16 JANUARY 2017 | DOI: 10.1038/NGEO2873

Large stationary gravity wave in the atmosphere of Venus

Tetsuya Fukuhara[1], Masahiko Futaguchi[2], George L. Hashimoto[3], Takeshi Horinouchi[4], Takeshi Imamura[5], Naomoto Iwagaimi[6], Toru Kouyama[7], Shin-ya Murakami[8], Masato Nakamura[8], Kazunori Ogohara[9], Mitsuteru Sato[4], Takao M. Sato[8], Makoto Suzuki[8], Makoto Taguchi[1]*, Seiko Takagi[10], Munetaka Ueno[11], Shigeto Watanabe[12], Manabu Yamada[13] and Atsushi Yamazaki[8]

The planet Venus is covered by thick clouds of sulfuric acid that move westwards because the entire upper atmosphere rotates much faster than the planet itself. At the cloud tops, about 65 km in altitude, small-scale features are predominantly carried by the background wind at speeds of approximately 100 m s^{-1}. In contrast, planetary-scale atmospheric features have been observed to move slightly faster or slower than the background wind, a phenomenon that has been interpreted to reflect the propagation of planetary-scale waves. Here we report the detection of an interhemispheric bow-shaped structure stretching 10,000 km across at the cloud-top level of Venus in middle infrared and ultraviolet images from the Japanese orbiter Akatsuki. Over several days of observation, the bow-shaped structure remained relatively fixed in position above the highland on the slowly rotating surface, despite the background atmospheric super rotation. We suggest that the bow-shaped structure is the result of an atmospheric gravity wave generated in the lower atmosphere by mountain topography that then propagated upwards. Numerical simulations provide preliminary support for this interpretation, but the formation and propagation of a mountain gravity wave remain difficult to reconcile with assumed near-surface conditions on Venus. We suggest that winds in the deep atmosphere may be spatially or temporally more variable than previously thought.

Akatsuki is a meteorological satellite investigating the atmospheric dynamics and cloud physics of Venus[1]. The Longwave Infrared Camera (LIR) and the Ultraviolet Imager (UVI) operate in the longest and shortest wavelength regions, respectively, among those of a suite of cameras on board Akatsuki[2]. Notable specifications of LIR are its spectral band of 8 to 12 μm, field of view of 16.4° × 12.4° covered by 328 × 248 pixels, noise equivalent temperature difference or temperature resolution of 0.3 K at a target temperature of 230 K, and absolute temperature accuracy of 3 K. LIR detects thermal radiation emitted from the cloud top. Since only a small fraction of solar irradiation is scattered in this wavelength region, Venus disk images taken by LIR show no clear boundary between the dayside and nightside hemispheres[3]. UVI has a field of view of 12.0° × 12.0° resolved by 1,024 × 1,024 pixels, and takes images of solar UV irradiation scattered by the cloud particles at the cloud top, from which the thermal radiation detected by LIR is emitted. The observable region is limited to the dayside. Two wavelength regions centred at 283 and 365 nm (with bandwidths of 15 nm), which correspond to the absorption bands of SO_2 and an unidentified absorber[4], respectively, are alternatively selectable.

Akatsuki was inserted into a Venus orbit on 7 December 2015 on the second attempt at Venus orbit insertion (VOI). Its four small thrusters—originally for attitude control—were used instead of the orbital manoeuvring engine, which was broken in the first attempt[5]. An observation sequence, which was scheduled to start five hours after the VOI operation, has allowed LIR and UVI to acquire the first Venus images at 05 h 26 m and 05 h 20 m UT, respectively. Fig. 1a shows the brightness temperature distribution of the cloud top retrieved from the image obtained by LIR. The brightness temperature represents the temperature in the altitude range centred at the cloud-top level of ∼65 km with a full-width at half-maximum of ∼10 km in the middle and low latitudes and in the lower regions of the high latitudes[6]. The most surprising and interesting feature is a huge bow-shaped structure extending from the northern polar region, crossing the equator and reaching the southern polar region. The end-to-end length of the bow-shaped structure is longer than 10,000 km. The bow-shaped structure consists of a high-temperature region, which splits into two high-temperature stripes at low latitude, and a low-temperature region located downstream of the high-temperature region. The highest

[1]College of Science, Rikkyo University, 3-34-1 Nishi-Ikebukuro, Toshima-ku, Tokyo 171-8501, Japan. [2]Omori Medical Center, Toho University, 6-11-1 Omorinishi, Ota-ku, Tokyo 143-8541, Japan. [3]Department of Earth Sciences, Okayama University, 3-1-1 Tsushimanaka, Kita-ku, Okayama 700-8530, Japan. [4]Faculty of Environmental Earth Science, Hokkaido University, N10W5, Sapporo, Hokkaido 060-0810, Japan. [5]Graduate School of Frontier Sciences, The University of Tokyo, 5-1-5 Kashiwanoha, Kashiwa, Chiba 277-8561, Japan. [6]School of Commerce, Senshu University, 2-1-1 Higashimita, Tama-ku, Kawasaki, Kanagawa 214-8580, Japan. [7]Artificial Intelligence Research Center, National Institute of Advanced Industrial Science and Technology, 2-3-26 Aomi, Koto-ku, Tokyo 135-0064, Japan. [8]Institute of Space and Astronautical Science, Japan Aerospace Exploration Agency, 3-1-1 Yoshinodai, Chuo-ku, Sagamihara, Kanagawa 252-5210, Japan. [9]School of Engineering, University of Shiga Prefecture, 2500 Hassaka, Hikone, Shiga 522-8533, Japan. [10]Research and Information Center, Tokai University, 4-1-1 Kitakaname, Hiratsuka, Kanagawa 259-1292, Japan. [11]Graduate School of Science, Kobe University, 7-1-48 Minatojima Minamimachi, Chuo-ku, Kobe, Hyogo 650-0047, Japan. [12]Space Information Center, Hokkaido Information University, Ebetsu, Hokkaido 069-8585, Japan. [13]Planetary Exploration Research Center, Chiba Institute of Technology, 2-17-1 Tsudanuma, Narashino, Chiba 275-0016, Japan. *e-mail: taguchi@rikkyo.ac.jp

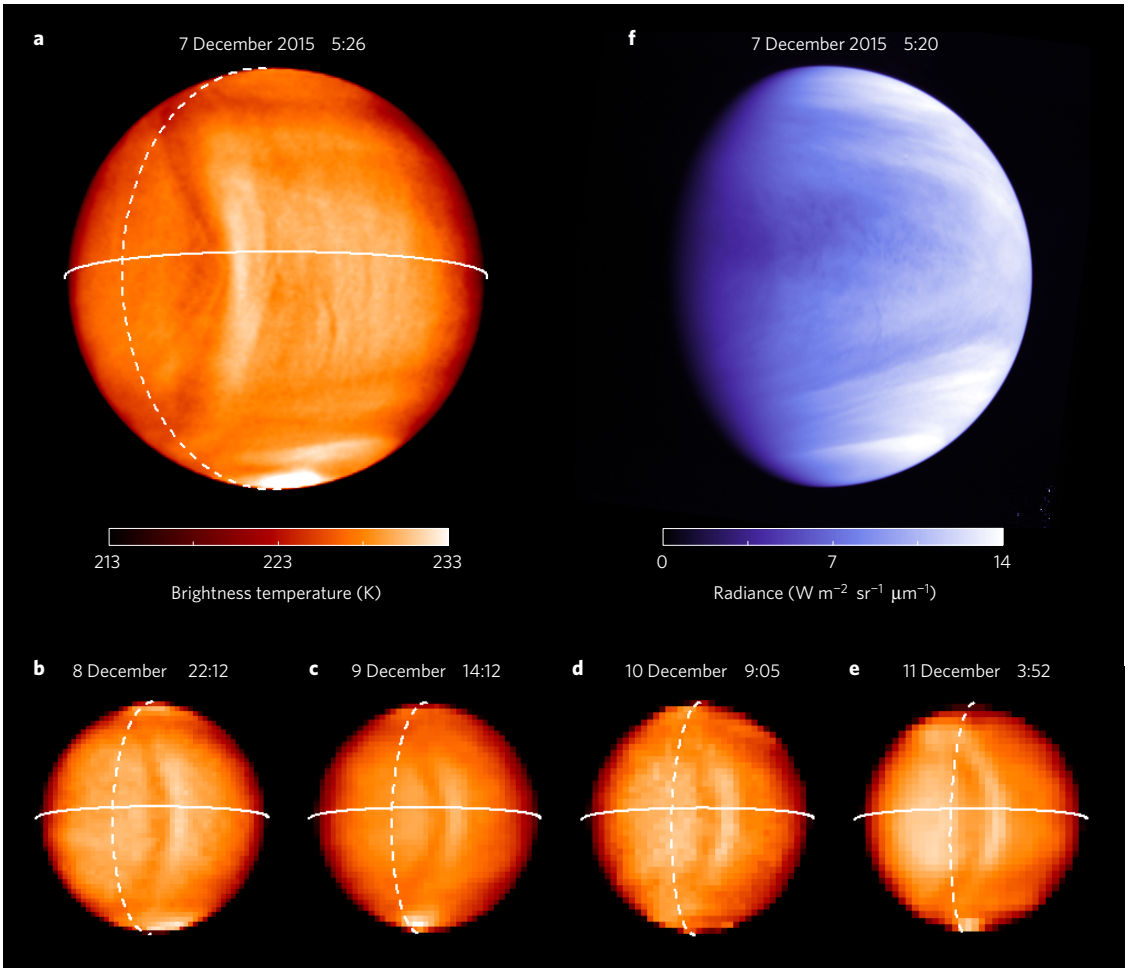

Figure 1 | Brightness temperature and UV brightness of the Venus disk. a–e, Sequence of brightness temperature distributions obtained by LIR from 7 December to 11 December 2015. The equator and evening terminator are shown by solid and dashed lines, respectively. The colour bar is valid only for **a**; the temperature ranges for **b–e** are adjusted so that the mean temperatures in a circle with a radius of 0.1 R_V at the disk centre are constant, where R_V is the Venus radius. **f**, UV brightness image obtained by UVI at a wavelength of 283 nm.

and lowest temperatures of the bow-shaped structure are 230–231 K and 225–226 K, respectively. Most of the structure is in the dayside, close to the evening terminator, shown by a dashed line in Fig. 1a, and appears symmetrical with respect to the equator.

The brightness temperature distributions of the cloud top obtained on 8–11 December 2015 are also shown in Fig. 1. Note that although the apparent diameter of the Venus disk decreased as the spacecraft moved away from Venus, the size of the Venus disk in Fig. 1b–e is adjusted to have the same diameter in each image. The bow-shaped structure existed for at least four days after 7 December while maintaining its shape, approaching the evening terminator day by day. Unfortunately, no data are available after 12 December because observation was suspended due to necessary operations related to the orbit, attitude and telecommunication of the spacecraft. When LIR observed the same longitude and local time region at the earliest opportunity on 15 January 2016, the bow-shaped structure had disappeared.

The bow-shaped structure appears dimly in the UV image at a wavelength of 283 nm. It can hardly be seen in Fig. 1f, as the contrast is much lower than that of the brightness temperature image. The bow shape is more difficult to identify in the 365 nm images, which are not shown here. Bow shapes have been observed in previous UV images of Venus[7]. A difference in the appearance between the bow shape observed in previous UV images and the bow shape newly found in the brightness temperature is that the former moves roughly at the speed of the super rotation[8].

The bow shape and surface topography

To investigate the position and motion of the bow-shaped structure in detail, the brightness temperature and the UV brightness derived from three successive images with an interval of a few hours were mapped to longitude–latitude coordinates and high-pass-filtered, as shown in Fig. 2. The accuracy of the longitude–latitude mapping was improved by fitting an ellipse to the observed limb of the Venus disk[9]. The bow-shaped structure in the brightness temperature map largely stayed above the same geographical position, and this is also true of the structure in the UV brightness map. The rotation period of Venus in the inertial coordinate system is −243 days. This value is negative because it rotates in the opposite direction to that of the Earth. When combined with the revolution period of 225 days, Venus has an angular velocity of rotation against the sun of $-3.1^\circ\ d^{-1}$. The ground speed of the bow-shaped structure is estimated to be $0.6 \pm 0.2^\circ\ d^{-1}$, indicating that the bow-shaped structure stayed at almost the same position above the ground rather than at the same local time. The Magellan global topography data record from the Planetary Data System (PDS) of NASA is smoothed by the running mean over 3° both in longitude and latitude, and shown in Fig. 2a. It is suggested that the centre of the bow-shaped structure is located at the western slope of the western highland of Aphrodite Terra, approximately 15° west of the peak in the surface topography.

Comparing Fig. 2a–c and Fig. 2d–f, it is found that the bright region of the bow-shaped structure in the UV image corresponds to

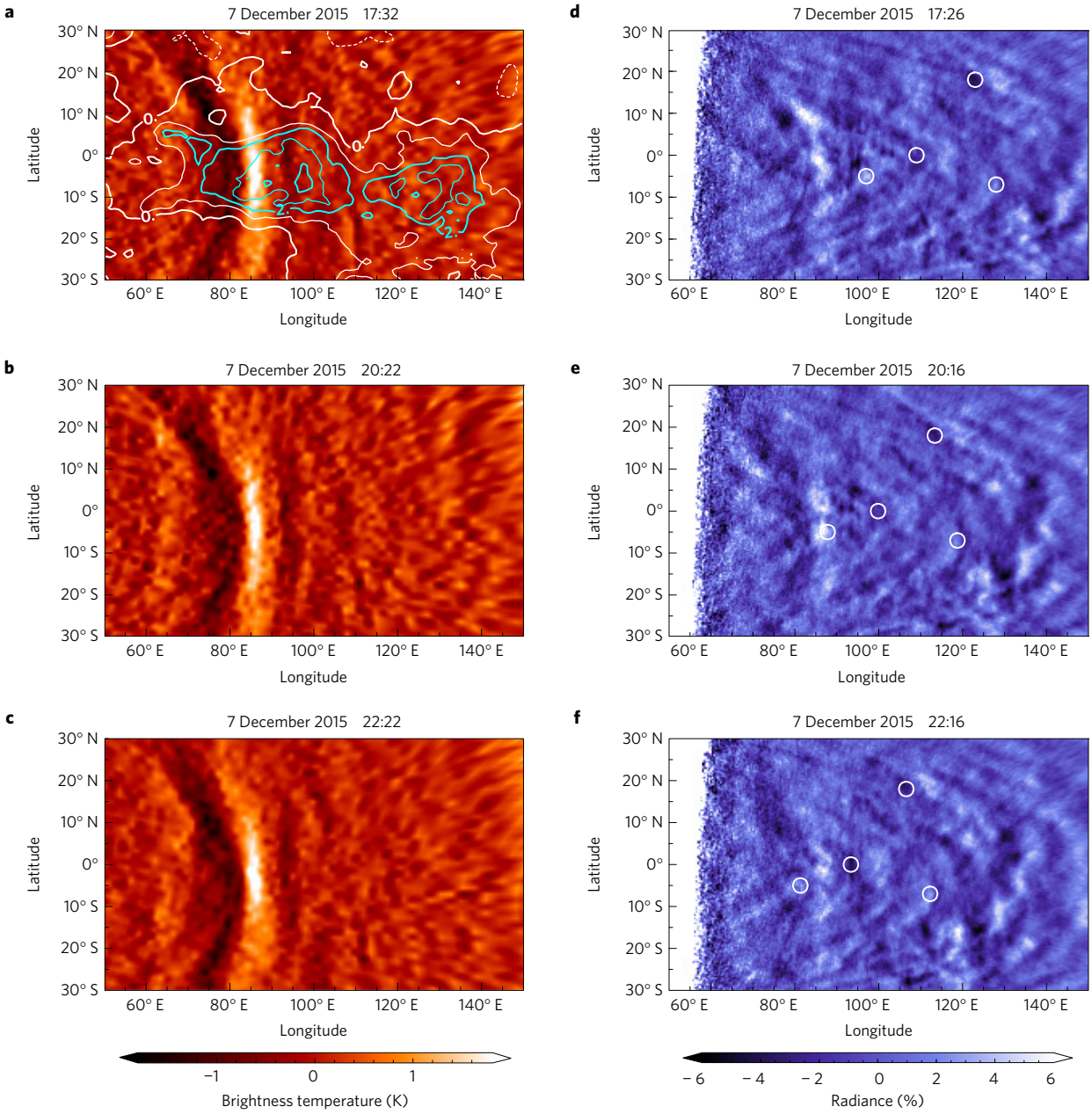

Figure 2 | High-pass-filtered brightness temperature and UV brightness at the cloud top of Venus. a–c, High-pass-filtered brightness temperature distributions derived from three successive shots by LIR with an interval of a few hours. The surface topography is overlaid by contour lines in **a** with units of km. Altitudes below 0 km are indicated by white dashed lines. **d–f**, UV brightness distributions acquired by UVI at a wavelength of 283 nm. The four small circles in each frame indicate the displacement of air parcels advected westwards at a zonal speed of −96 m s^{-1}.

the high-temperature region. Moreover, smaller-scale bow-shaped structures are identified both in the brightness temperature and in the UV brightness maps as meridionally aligned dark filaments. As an example, one of them stayed at the same location (110° E, −20° S). At the same time, advection of the small-scale features is clearly seen in the sequence of UV images, as demonstrated by four arbitrarily placed circles that move westwards at a speed of −96 m s^{-1} (Fig. 2d–f). By tracking the distinct Y-shaped structures using a cloud-tracking technique[10], areal mean zonal wind velocities in the latitude region between ±15° on 7–9 December are derived to be −96, −96 and −107 m s^{-1}, respectively, with a spatial standard deviation of several m s^{-1}.

After the bow shape appeared in December 2015, no similar prominent features were observed except for very weak events detected in the brightness temperature maps on 15 and 26 April 2016 and 6 and 26 May 2016. Their horizontal scale and meridionally aligned bow-shaped appearance are similar to those of the event in December 2015, but the amplitudes are less than 1 K.

Stationary gravity wave

Given the shape and the fast speed relative to the background super rotation, the only reasonable interpretation of the stationary bow shape is that it is induced by an atmospheric gravity wave packet. A study[11] has proposed that the long-term mean zonal wind distribution estimated from the UV images obtained by the Venus Monitoring Camera on board Venus Express is caused by non-uniform momentum forcing by stationary gravity waves generated by mountain airstreams at ground level. It is implicitly assumed that the waves have small scales, as parameterized in climate models for the Earth[12]. The present study shows direct evidence of the existence

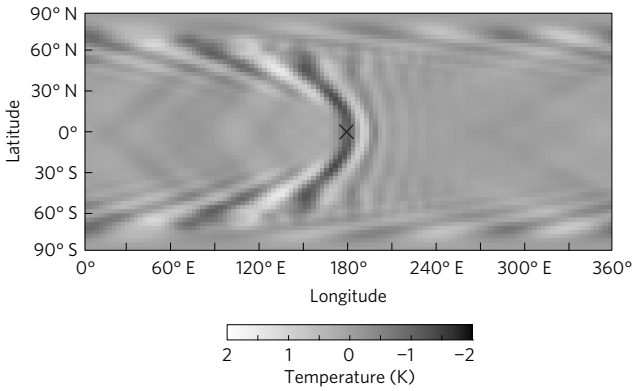

Figure 3 | Disturbance temperature field at 65 km altitude associated with a stationary gravity wave calculated by a numerical model. The model solves upward propagation of a gravity wave packet excited by a stationary geopotential disturbance at the bottom boundary of 10 km altitude. The forcing is located at the centre of this plot is indicated by the cross, and has a half-width of ∼6° in longitude and latitude. The direction of the background zonal wind (super rotation) is from right to left.

of stationary gravity waves, and it further shows that such stationary gravity waves can have a very large scale—perhaps the greatest ever observed in the solar system.

The bow-shaped structure identified in the UV brightness is explained by a perturbation in the column abundance of UV absorber due to the passage of a gravity wave. UV-absorber-rich air may be supplied in an upwelling region, where the temperature is lower than that of the surrounding area due to adiabatic cooling.

From conventional knowledge of the Venusian atmosphere[13], the formation and propagation of such mountain waves appear difficult. Convection in the observed statically, near-neutral layers between the cloud-top level and the ground[14] can disturb gravity wave propagation. The long-term angular momentum balance in the presence of meridional circulation requires that the mean surface wind in the low-latitude region is against the solid planet rotation, as in the Earth's atmosphere. In that case, there exists a critical level above the surface beyond which stationary gravity waves cannot propagate through. Since the critical-level filtering is fatal, our result may suggest the existence of some spatial or temporal variability in the distribution of winds in the lower atmosphere, which might be why huge gravity waves are not always observed.

A numerical model is used to simulate pattern formation induced by gravity waves excited in the lower atmosphere. In the model, a Gaussian-shaped, stationary geopotential forcing with a half-width of ∼6° is imposed at a longitude of 180° on the equator at a bottom altitude of 10 km, and the disturbance excited by it is calculated up to 96 km under a realistic basic state (see Methods). The bottom height of 10 km enables us to avoid the problem of a possible critical layer in the lowest atmosphere. Figure 3 shows the steady-state disturbance temperature field at ∼65 km altitude. The localized forcing at the bottom generates a gravity wave packet with a bow shape, which is typical of a gravity wave generated by an isolated mountain[15]. The latitudinal extent of the wave packet increases with height, growing to a planetary scale at the cloud-top level, below which the vertical wavelength is around 30 km. The maximum amplitude at low latitude occurs just above the forcing. The resemblance of the model result to the observation is remarkable.

Both the zonal wind speed and static stability are small below 10 km, so the condition of wave generation and propagation is sensitive to their small changes, which is why we limited our simulation to altitudes above 10 km. More elaborate modelling is left for future studies. Since gravity waves transfer momentum, mountain-induced waves may be important for the climatology of Venus.

Methods

Methods, including statements of data availability and any associated accession codes and references, are available in the online version of this paper.

Received 25 August 2016; accepted 8 December 2016; published online 16 January 2017

References

1. Nakamura, M. *et al*. Overview of Venus Orbiter, Akatsuki. *Earth Planets Space* **63,** 443–457 (2011).
2. Fukuhara, T. *et al*. LIR: Longwave Infrared Camera onboard the Venus Orbiter Akatsuki. *Earth Planets Space* **63,** 1009–1018 (2011).
3. Taguchi, M. *et al*. Characteristic features in Venus' nightside cloud-top temperature obtained by Akatsuki/LIR. *Icarus* **219,** 502–504 (2012).
4. Esposito, L. W. *et al*. in *Venus* (eds Hunten, D. M., Colin, L., Donahue, T. M. & Moroz, V. I.) 484–564 (Univ. Arizona Press, 1983).
5. Nakamura, M. *et al*. AKATSUKI returns to Venus. *Earth Planets Space* **68,** 75 (2016).
6. Taguchi, M. *et al*. Longwave Infrared Camera onboard the Venus Climate Orbiter. *Adv. Space Res.* **40,** 861–868 (2007).
7. Rossow, W. B. *et al*. Cloud morphology and motions from Pioneer Venus images. *J. Geophys. Res.* **85,** 8107–8128 (1980).
8. Del Genio, A. D. & Rossow, W. B. Planetary-scale waves and the cyclic nature of cloud top dynamics on Venus. *J. Atmos. Sci.* **47,** 293–318 (1990).
9. Ogohara, K. *et al*. Automated cloud tracking system for the Akatsuki Venus Climate Orbiter data. *Icarus* **217,** 661–668 (2012).
10. Ikegawa, S. & Horinouchi, T. Improved automatic estimation of winds at the cloud top of Venus using superposition of cross-correlation surfaces. *Icarus* **271,** 98–119 (2016).
11. Bertaux, J.-L. *et al*. Influence of Venus topography on the zonal wind and UV albedo at cloud top level: the role of stationary gravity waves. *J. Geophys. Res.* **121,** 1087–1101 (2016).
12. Lindzen, R. S. Turbulence and stress owing to gravity wave and tidal breakdown. *J. Geophys. Res.* **86,** 9707–9714 (1981).
13. Schubert, G. in *Venus* (eds Hunten, D. M., Colin, L., Donahue, T. M. & Moroz, V. I.) 681–765 (Univ. Arizona Press, 1983).
14. Seiff, A. *et al*. Measurements of thermal structure and thermal contrasts in the atmosphere of Venus and related dynamical observations: results from the four Pioneer Venus probes. *J. Geophys. Res.* **85,** 7903–7933 (1980).
15. Smith, R. B. Linear theory of stratified hydrostatic flow past an isolated mountain. *Tellus* **32,** 348–364 (1980).

Acknowledgements

We would like to acknowledge all the members of the Akatsuki project team for their efforts in the Akatsuki operation, which led to the successful VOI. This work was supported by JSPS KAKENHI Grant Numbers JP15K17767 and JP16H02231.

Author contributions

M.T. and S.W. are the principal investigators of LIR and UVI, respectively. T.F., M.F., G.L.H., T.I., N.I., T.K., M.N., M.S., T.M.S., M.S., S.T. and M.U. are co-investigators of LIR. M.Y. and A.Y. are co-investigators of UVI. T.H., S.-y.M. and K.O. contributed to the derivation of the wind field. T.I. contributed to the numerical modelling.

Additional information

Reprints and permissions information is available online at www.nature.com/reprints. Correspondence and requests for materials should be addressed to M.T.

Competing financial interests

The authors declare no competing financial interests.

Methods

High-pass filtering. Figure 2 shows high-pass filtered brightness temperature and UV radiance obtained as the anomaly from the 15° running mean along the longitude. Prior to the high-pass filtering, the UV radiance is divided by $\cos\theta_z$, where θ_z is the local solar zenith angle, to correct for the θ_z dependence of the solar irradiation. The data for which $\cos\theta_z < 0.05$ are not shown, because the error is larger than natural variations.

Derivation of wind fields. The cloud tracking was conducted using a digital tracking method with good quality control[9]. For each day from 7 to 9 December, tracking was made with three UV images at 365 nm with time intervals of two to three hours. Tracking was also made with images at 283 nm, and the results were consistent.

Numerical simulation. The numerical model used to solve the propagation of a stationary gravity wave is a nonlinear primitive equation model in spherical geometry similar to one developed in a previous work[16]. The model covers the Venusian atmosphere from 10 km (47.39×10^5 Pa) to ~96 km (47.39×10^{-1} Pa). The basic zonal wind and temperature profiles on the equator are given by polynomial functions used in a previous work[17] based on *in situ* observations by entry probes. The zonal wind speed is 8 m s^{-1} at 10 km, increasing monotonically to 94 m s^{-1} at 68 km. As for the zonal wind above, the average of the model A (strong shear above the cloud top) and model B (no shear above the cloud top) profiles defined in the work is adopted. Mid-latitude jets relative to the solid-body rotation are introduced into the model, resulting in a roughly constant zonal wind in the latitudinal range of 45° S–45° N at each altitude. The meridional distribution of the basic temperature is calculated from the basic zonal wind and the equatorial temperature profile assuming cyclostrophic balance. The static stability is positive everywhere, in contrast to the actual Venusian atmosphere, where neutral stratification is observed around 50–55 km altitude. Even in the presence of the neutral stability layer, the wave would still propagate up to the cloud-top level, because the locally evanescent character of the wave in the layer would not totally remove the wave energy above the layer. A geopotential forcing is imposed on the bottom boundary with a Gaussian-shaped function: $60 \times \exp[-(\delta\lambda^2 + \delta\theta^2)/(6^\circ)^2]$ m^2 s^{-2}, where $\delta\lambda$ and $\delta\theta$ are the longitudinal and latitudinal distances from the centre of the forcing, respectively. The centre of the forcing is located at a longitude of 180° on the equator. Dissipation due to radiative damping is represented by Newtonian cooling with a time constant of $20 \times \exp[-(z-60)/10]$ Earth days, where z is the altitude in kilometres, based on radiative transfer modelling[18]. Altitudes above 85 km comprise a sponge layer that suppresses wave reflection by attenuating the disturbance temperature and wind velocity at a rate that is twice the radiative damping rate. Since the development of the background atmosphere is beyond the scope of this study, the wind velocity and the temperature are divided into their zonal mean and disturbance, and the former is set to the basic state at each time step. The grid interval is 3°, both in longitude and latitude, and the vertical coordinate is represented by 100 pressure levels with a constant spacing in log pressure. The momentum and thermodynamic equations are integrated using a centred flux-form space difference, Euler backward (Matsuno) scheme until a quasi-steady state is achieved, with the continuity and hydrodynamics equations being used at each time step to diagnose the vertical velocity and the geopotential with boundary conditions.

Code availability. We have opted not to make the computer codes used in the cloud-tracking analysis and numerical modelling of the gravity wave available.

Data availability. The data that support the findings of this study will be available at Data ARchives and Transmission System (DARTS) of ISAS/JAXA (http://darts.isas.jaxa.jp) and at the PDS of NASA (https://pds.nasa.gov).

References

16. Imamura, T. Meridional propagation of planetary-scale waves in vertical shear: implication for the Venus atmosphere. *J. Atmos. Sci.* **63,** 1623–1636 (2006).
17. Schubert, G. & Walterscheid, R. L. Propagation of small-scale acoustic-gravity waves in the Venus atmosphere. *J. Atmos. Sci.* **41,** 1202–1213 (1984).
18. Crisp, D. Radiative forcing of the Venus mesosphere II. Thermal fluxes, cooling rates, and radiative equilibrium temperatures. *Icarus* **77,** 391–413 (1989).